Volume 10 | Number 17 | 7 May 2018 | Pages 7873–8340

Nanoscale

rsc.li/nanoscale

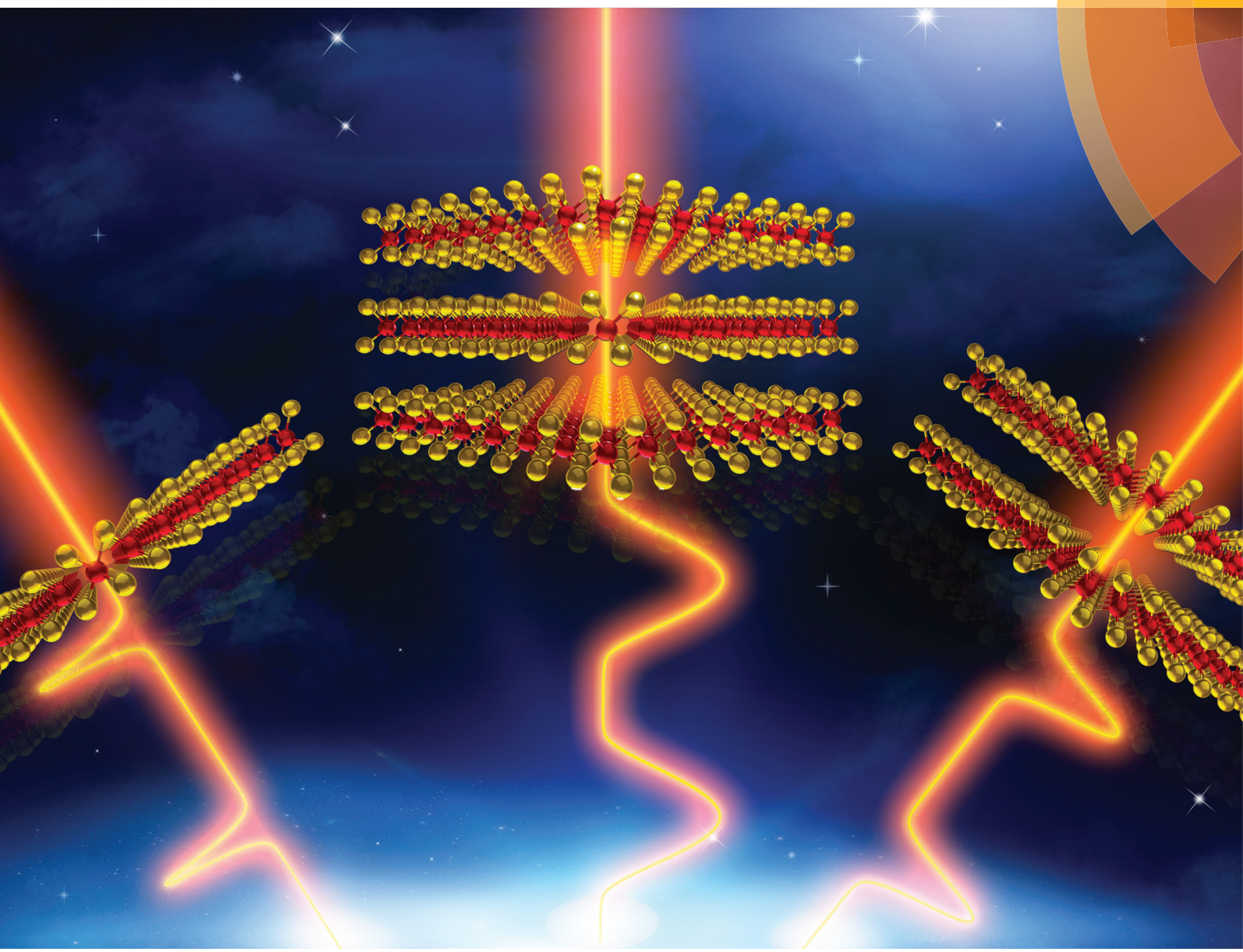

ISSN 2040-3372

ROYAL SOCIETY OF CHEMISTRY

PAPER
Ming Lei, Peiguang Yan, Zhiyi Wei *et al.*
Tungsten diselenide for all-fiber lasers with the chemical vapor deposition method

NCNST

Nanoscale

PAPER

View Article Online
View Journal | View Issue

Cite this: *Nanoscale*, 2018, **10**, 7971

Tungsten diselenide for all-fiber lasers with the chemical vapor deposition method

Wenjun Liu,[a,b] Mengli Liu,[a] Jinde Yin,[c] Hao Chen,[c] Wei Lu,[d] Shaobo Fang,[b] Hao Teng,[b] Ming Lei,*[a] Peiguang Yan *[c] and Zhiyi Wei*[b]

Received 17th January 2018,
Accepted 25th February 2018

DOI: 10.1039/c8nr00471d

rsc.li/nanoscale

Two-dimensional materials have become the focus of research for their photoelectric properties, and are employed as saturable absorption materials. Currently, the challenge is how to further improve the modulation depth of saturable absorbers (SAs) based on two-dimensional materials. In this paper, three kinds of WSe_2 films with different thicknesses are prepared using the chemical vapor deposition method. The nonlinear optical responses of the WSe_2 films including the nonlinear saturable absorption and nonlinear refractive index are characterized by the double-balanced detection method and *Z*-scan experiments. Different modulation depths are successfully obtained by controlling the thickness of the WSe_2 films. We further incorporate them into an all-fiber laser to generate mode-locked pulses. The mode-locked fiber lasers with a pulse duration of 185 fs, 205.7 fs and 230.3 fs are demonstrated when the thickness of the WSe_2 films is measured to be 1.5 nm, 5.7 nm and 11 nm, respectively. This work provides new prospects for WSe_2 in ultrafast photonic device applications.

Introduction

Graphene, with its unique two-dimensional (2D) layered structure, has promoted the study of 2D materials in the field of optoelectronics.[1–3] As a new type of material, 2D materials have been used to generate laser pulses because of their excellent saturable absorption characteristics and ultrafast dynamics related to their special band structure.[4–9] The 2D materials with wide bandwidth, low loss, high damage threshold, ultrafast response time and large modulation depth have attracted much attention from researchers.[10–13]

On the other hand, the passive mode-locking technique, which is one of the most important techniques to achieve ultrashort pulses, has been applied in modern optics and optoelectronics.[14–18] SAs are a key component for the passively mode-locked fiber laser. The use of SAs has become an effective approach to accumulate enough nonlinear phase shift without lengthening the cavity of fiber lasers.[19–21] Therefore, some materials with the saturable absorption property are becoming a research focus in ultrafast optics.[22–27]

Transition metal dichalcogenides (TMDs) are confirmed as emerging and promising saturable absorption materials.[28,29] The monolayer of TMDs, which consists of a layer of transition metal atoms (such as Mo or W) sandwiched between two layers of sulfur atoms (usually S, Se or Te), is bonded with neighbour layer by the weak Van der Waals interaction.[30,31] Bulk TMDs have been practicably exfoliated into filmy nanosheets due to the development of electro-optic devices with remarkable performance.[32–35] Meanwhile, exfoliating a single crystal of a few layers from the bulk sample results in changes of the bandgap.[36–39] Researchers have indicated that TMDs exhibit complementary properties compared with graphene.[40] In previous studies, WS_2 and MoS_2 were the most reported materials in cases when TMDs were employed as SAs. The Q-switched or mode-locked fiber lasers based on MoS_2 and WS_2 SAs at multifarious operating wavelengths have been widely implemented.[41–46] As the analogue of WS_2 and MoS_2, tungsten diselenide (WSe_2) has a similar molecular structure, broadband absorption characteristic and relatively small bandgap.[47–50]

However, WSe_2 remains at an early stage of development, and it is rare to investigate the optical properties of WSe_2 in mode-locked fiber lasers. Although WSe_2–polyvinyl alcohol (PVA) is used in the preparation of SAs, they are easily damaged by lasers due to the presence of dopants in the materials.[50] Besides, the scattering of nanomaterials leads to additional thermal dissipation, and limits the damage

[a]*State Key Laboratory of Information Photonics and Optical Communications, School of Science, P. O. Box 91; Beijing University of Posts and Telecommunications, Beijing 100876, China. E-mail: mlei@bupt.edu.cn*
[b]*Beijing National Laboratory for Condensed Matter Physics, Institute of Physics, Chinese Academy of Sciences, Beijing 100190, China. E-mail: zywei@iphy.ac.cn*
[c]*Shenzhen Key Laboratory of Laser Engineering, College of Optoelectronic Engineering, Shenzhen University, Shenzhen 518060, China. E-mail: yanpg@szu.edu.cn*
[d]*University Research Facility in Materials Characterization and Device Fabrication, Hong Kong Polytechnic University, Kowloon, Hong Kong*

threshold of SAs. Moreover, the modulation depth is small; this characteristic is not conducive to the realization of self-starting ultrashort fiber lasers.[50] Therefore, it is one of the hot research subjects to further improve the laser induced damage threshold and modulation depth of SAs based on 2D materials.

In this paper, three kinds of WSe_2 films with different thicknesses are investigated. The chemical vapor deposition (CVD) method is adopted to prepare high quality films of WSe_2. Because WSe_2 is suitable for high power and high temperature applications, it does not need to be doped into PVA or polymethyl methacrylate (PMMA) when WSe_2 is transferred onto the end face of optical fiber ferrules. Besides, few-layer/multilayer materials can be easily prepared by the CVD method, and the modulation depth can be increased by layer number control. Thus, the modulation depth of SAs is improved. The enhancement of the WSe_2 SA performance leads to the realization of a stable mode-locked all-fiber laser, which has the shortest pulse duration and highest signal-to-noise ratio (SNR) in the same type of all-fiber laser based on TMDs. We believe that our approaches are beneficial for the improved performance of the WSe_2 SA, and promote the applications of 2D materials in optical modulation devices.

Results and discussion

WSe_2 SA fabrication and characterization

In the experiment, large area and high lattice quality few-layer WSe_2 films are grown on an Al_2O_3 substrate by the CVD method. Firstly, Se powder (0.04 g) is placed at the input port of Ar/H_2 in the furnace, and the heating temperature is maintained at 270 °C in the CVD process. The WO_3 powder (0.25 g) is placed behind the Se powder in the direction of the Ar/H_2 input port. During the CVD process, the WO_3 powder is heated to 920 °C at a ramp rate of 25 °C min^{-1}. When the temperature of the WO_3 powder reaches 920 °C, we keep it for 15 minutes at this temperature so that large area and high lattice quality few-layer WSe_2 films grow on the Al_2O_3 substrate. Finally, the furnace is allowed to cool naturally, and the sample can be taken out after it reaches room temperature.

Using the PMMA, the WSe_2–PMMA composites are stripped out from the Al_2O_3 substrate. And then, the PMMA on the WSe_2 films is removed by using acetone. Besides, the WSe_2 films are processed with deionized water to remove the PMMA residue as shown in Fig. 1(a). The free-standing WSe_2 films are finally transferred onto the end face of the optical fiber ferrule as seen in Fig. 1(b). The WSe_2 films, optical fiber ferrules and adapter are integrated to form the WSe_2 SA devices as shown in Fig. 1(c).

X-ray photoelectron spectroscopy (XPS), as an effective technology to determine the elemental composition of a sample, has been employed in characterizing the chemical performance of WSe_2 in Fig. 2. The peaks at 32.56 eV and 34.86 eV are assigned to W $4f^{7/2}$ and W $4f^{5/2}$ binding energies, respectively, in Fig. 2(a), which corresponds to W^{4+}.[51] The

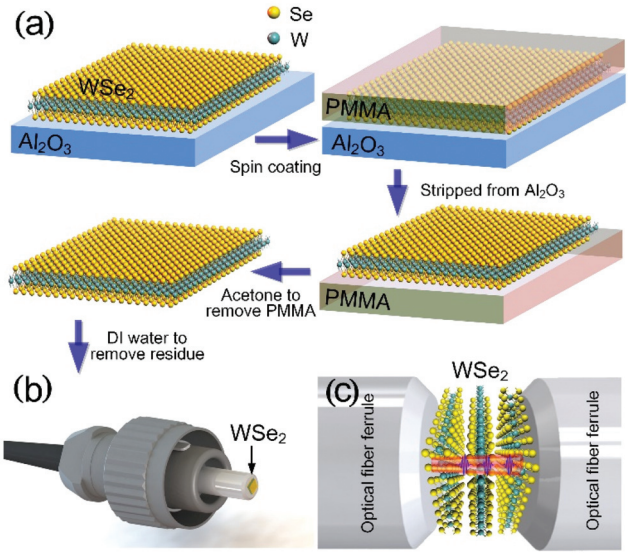

Fig. 1 Schematic representation of the preparation of the WSe_2-based SA. (a) The transfer process of WSe_2 films. (b) Photograph of WSe_2 films on the end face of the optical fiber ferrule. (c) Illustration of the interaction between light and few-layer WSe_2.

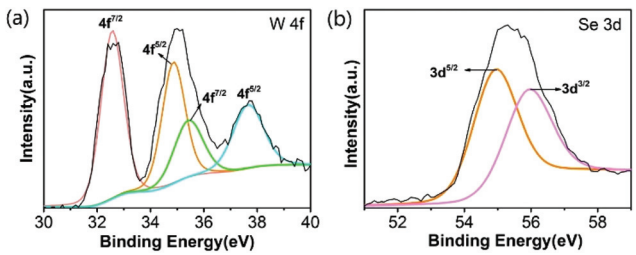

Fig. 2 The X-ray photoelectron spectroscopy of WSe_2 films. (a)The XPS spectrum of W 4f; (b) The XPS spectrum of Se 3d.

peaks of the Se region at 54.9 eV and 56 eV are assigned to $3d^{5/2}$ and $3d^{3/2}$, respectively, in Fig. 2(b). This indicates that the WSe_2 film has been successfully prepared.

To nondestructively determine the lattice dynamics of the WSe_2 SA, Raman spectroscopy which has played an important role in the characterization of 2D materials is the preferred technology to adopt. Different from other TMDs which possess a well separation between the E_g and A_g modes, the most significant Raman peaks which correspond to the $E_{2g}{}^1$ modes of WSe_2 are clustered around 250 cm^{-1} in Fig. 3(a). According to previous studies, a new mode A_{1g} appears at 5–11 cm^{-1} after the main peak when the sample has less than four layers.[52,53] Transmission electron microscopy (TEM) as one of the most effective imaging techniques has been used to further research the microstructure of 2D materials. When the length of scale bar is 1 nm, the uniform arrangement of W and Se atoms is presented in Fig. 3(b), which corresponds to the theoretical model of the microstructure of WSe_2.

Atomic force microscopy (AFM) provides the 3D imaging of samples such as surface topography and surface roughness at

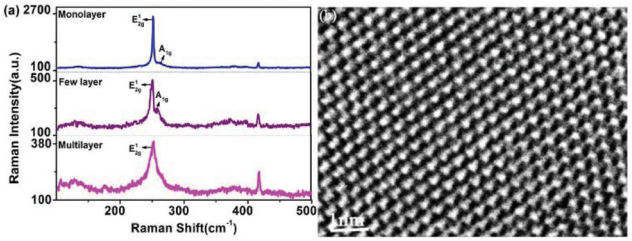

Fig. 3 Characterization of the WSe_2 sample. (a) Raman spectrum of the WSe_2 sample. (b) TEM image of the WSe_2 sample.

nanoscale resolution under native conditions as shown in Fig. 4(a)–(c). The altitude difference of the surface topography indicates that the thicknesses of the WSe_2 films are 1.5 nm, 5.7 nm and 11 nm. According to the double-balanced detection method, a relationship between the transmittance of the material and the intensity of power can be obtained. It can be seen from the experimental data points that the sample exhibits a lower transmittance at low power and a higher transmittance at high power, which is consistent with the typical property of SAs. As shown in Fig. 4(d)–(f), the modulation depths of the 1.5 nm thick, 5.7 nm thick and 11 nm thick WSe_2 SAs are 52.38%, 47.38% and 34.41%, respectively.

The changing trends of the film thickness and modulation depth are opposite to each other. We believe there are two reasons for the large modulation depth of the CVD-grown WSe_2. On the one hand, the CVD method can achieve better uniformity of the WSe_2 films. In ref. 54, the authors have also claimed that a good uniformity can result in a high modulation depth of materials. On the other hand, the layered WSe_2 exhibits thickness-dependent transition from the direct bandgap in the monolayer to the indirect gap in the bulk. When the number of layers of WSe_2 increases, the scattering in multilayer materials will enhance as it discussed in ref. 1. It will lead to the nonsaturated loss, which makes the modulation depth decrease. Therefore, the thinner the WSe_2 films are, the larger the modulation depth of the WSe_2-based SA becomes.

Z-Scan experiments of the WSe_2 sample in the near-infrared band

The nonlinear optical response of WSe_2 including the absorption coefficient and nonlinear refractive index is characterized by *Z*-scan experiments. WSe_2 films are excited by mode-locked lasers with a pulse duration of 25 ps and a repetition rate of 1 kHz at 1064 nm. The incident laser can be separated into two beams by the beam splitter; one of them is used for direct detection to ensure the stability of light intensity, and the other is tightly focused by the objective lens to obtain the nonlinear optical properties of the sample. The WSe_2 sample moving around the focal point of the lens can be regarded as a kind of lens-like medium due to the nonlinearity of the medium and the transverse spatial inhomogeneity of the Gaussian beam, which will eventually lead to the divergence or convergence of the beam, and change the transverse distribution of the far-field light field. With an appropriate aperture placed in the far field, the optical power through the aperture can be measured when the sample is in different positions. Open-aperture (OA) *Z*-scans that reflect the nonlinear absorption of WSe_2 can be realized when the diaphragm is fully open. The closed-aperture (CA) *Z*-scans, which are used to measure the nonlinear refractive index, can be obtained with the small diaphragm aperture.

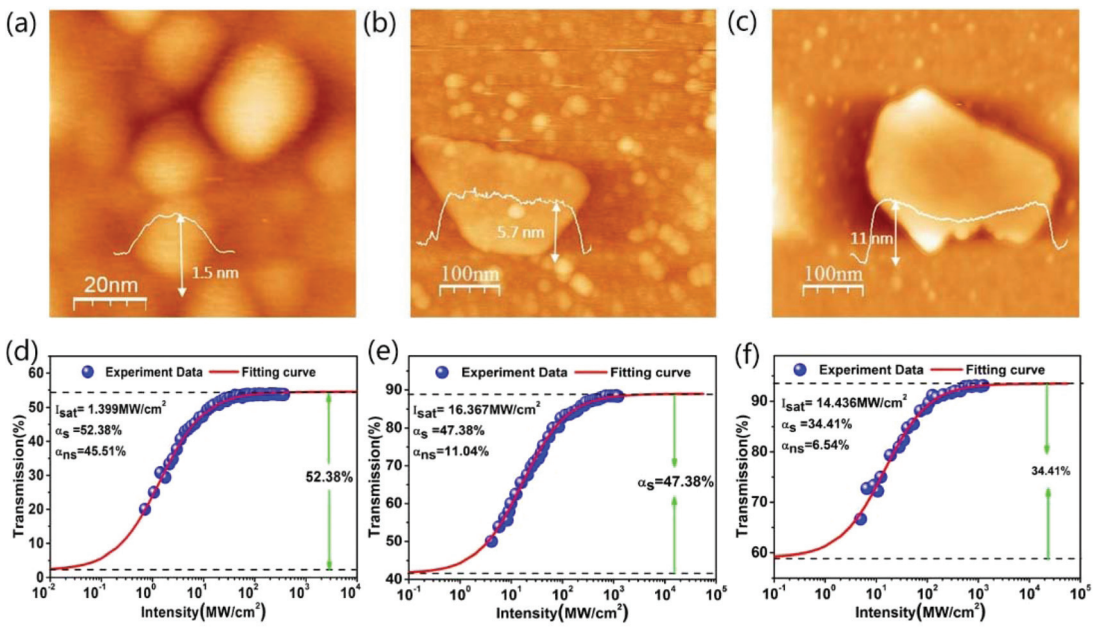

Fig. 4 (a)–(c) Morphology of WSe_2 measured with AFM. (d)–(f) Power dependent nonlinear saturable absorption of the WSe_2 SA.

Assuming the Gaussian beam translated along the Z-axis, the magnitude of $E(z,r,t)$ can be expressed as

$$E(z,r,t) = E_0(t)\frac{\omega_0}{\omega(z)}\exp\left(-\frac{r^2}{\omega^2(z)} - \frac{ikr^2}{2R(z)}\right)e^{-i\phi(z,t)},$$

where $\omega^2(z) = {\omega_0}^2(1 + z^2/{z_0}^2)$ is the beam radius at z, $R(z) = z(1 + {z_0}^2/z^2)$ is the curvature radius, $z_0 = k{\omega_0}^2/2$ is the beam diffraction length, $k = 2\pi/\lambda$ is the wave vector, λ is the laser wavelength, $E_0(t)$ is the electric field at focus, and ω_0 is the focus radius. It is assumed that the Rayleigh length of the focused beam is much longer than the sample thickness, which is called the thin sample approximation. The change of the nonlinear phase shift $\Delta\phi$ will be obtained by

$$\Delta\phi(z,r,t) = \Delta\phi_0(z,t)\exp\left(-\frac{2r^2}{\omega^2(z)}\right),$$

where $\Delta\phi_0(z,t) = \dfrac{\Delta\phi_0(t)}{1 + z^2/{z_0}^2}$, $\Delta\phi_0(t) = kn_2I_0L_{\text{eff}}$ with I_0 is the irradiance within the sample, $L_{\text{eff}} = (1 - e^{-\alpha L})/\alpha$ is the effective length of the sample, L is the sample length, and α is the linear absorption coefficient. For the OA Z-scan, we can calculate the normalized Z-scan transmittance $T(z)$ as

$$T(z,t) = \frac{\int_0^{r_a}|E_a(\Delta\phi_0,r,z,t)|^2 r\mathrm{d}r}{S\int_0^{\infty}|E_a(0,r,z,t)|^2 r\mathrm{d}r},$$

where E_a represents the electric-field profile at the aperture while r_a is the aperture radius, and $S = 1 - \exp\left(-\dfrac{2{r_a}^2}{{\omega_a}^2}\right)$ is the aperture transmittance in the linear regime. As shown in Fig. 5(a), (c) and (e), a sharp absorption peak can be observed at coordinate $z = 0$, which clearly reveals the nonlinear absorption property of WSe_2. The typical Z-scan measurement fitting curve of CA/OA is shown in Fig. 5(b), (d) and (f); the graphic features of the pre-focal peak and post-focal valley indicate the self-defocusing characteristics with the negative nonlinear refractive index. The CA/OA Z-scan curve traced by experimental data points shown above is fitted through the formula[55]

$$T(x) = 1 + \frac{4x\Delta\phi_0(t)}{(1+x^2)(9+x^2)} + \frac{4(3x^2-5)\Delta{\phi_0}^2(t)}{(1+x^2)^2(9+x^2)(25+x^2)} + \frac{32(3x^2-11)x\Delta{\phi_0}^3(t)}{(1+x^2)^3(9+x^2)(25+x^2)(49+x^2)},$$

where $T(x)$ is the normalized transmittance, $x = z/z_0$, and z represents the longitudinal displacement of the sample from the focus ($z = 0$). Meanwhile, based on $n_2 = \Delta\phi_0(t)/kI_0L_{\text{eff}}$, the refractive index n_2 will be deduced. The nonlinear absorption coefficient of WSe_2 is estimated as $\sim -8.82 \times 10^{-9}$ cm^2 W^{-1}, $\sim -3.77 \times 10^{-9}$ cm^2 W^{-1} and $\sim -2.07 \times 10^{-9}$ cm^2 W^{-1} according to the actual experimental data points with a sample thickness of 1.5 nm, 5.7 nm and 11 nm, respectively.

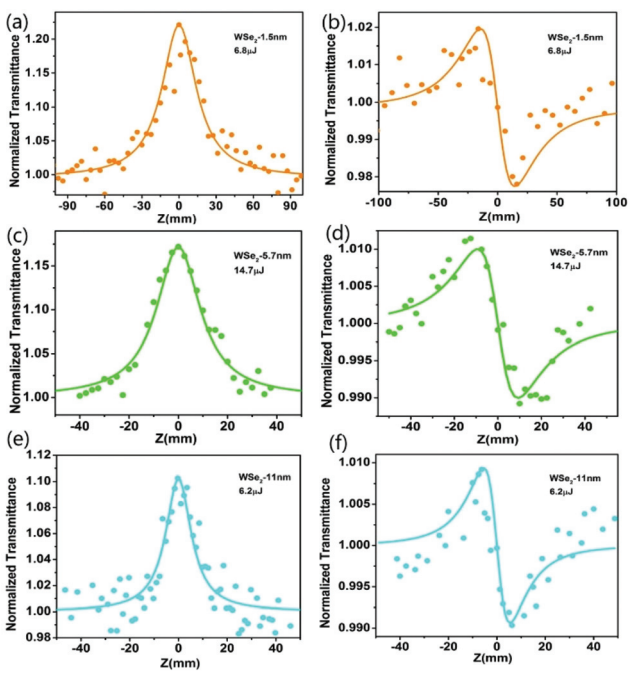

Fig. 5 (a), (c), (e) The OA Z-scan. (b), (d), (f) The CA/OA Z-scan. The curves of the WSe_2 films are under the excitation of 25 ps pulses at 1064 nm.

Experimental

The schematic diagram of the all-fiber mode-locked Er-doped fiber laser (EDF) laser is illustrated in Fig. 6. The total length of the ring cavity is about 3.8 m. The EDF is counter pumped through a 980/1550 nm wavelength division multiplexing (WDM) coupler with two SMF-28e fiber pigtails. A 35 cm long high gain EDF (Liekki 110-4/125) is used as the gain medium with a group velocity dispersion (GVD) of 12 fs^2 m^{-1}. A polarization independent isolator is inserted into the cavity to force the unidirectional operation, and an intra-cavity polarization controller (PC) is used to fine-tune the linear polarization state. A 20% fiber coupler with an SMF-28e fiber pigtail is used to export the laser signal. The WSe_2 films with the thickness of 1.5 nm, 5.7 nm and 11 nm are transferred onto the end face of optical fiber ferrules. A fiber adapter and two optical fiber ferrules with WSe_2 films are integrated to form the WSe_2 SA devices. An optical spectrum analyzer and a 500 MHz

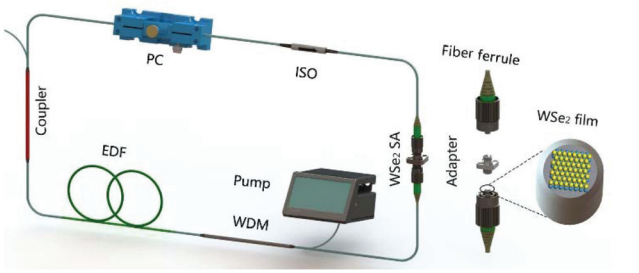

Fig. 6 Schematic diagram of the all-fiber mode-locked EDF laser based on the WSe_2-based SA.

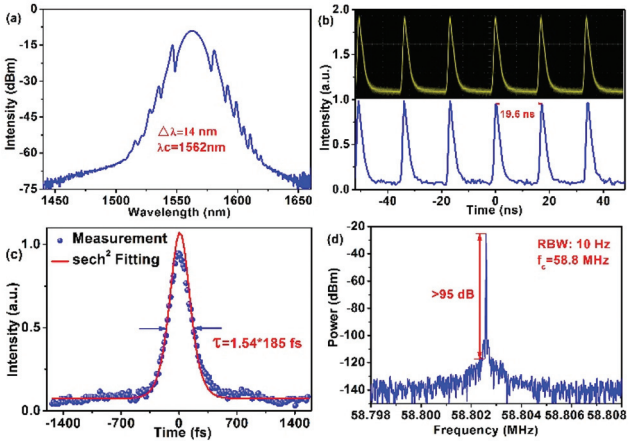

Fig. 7 Experimental results of the all-fiber mode-locked EDF laser with the 1.5 nm thick WSe_2-based SA. (a) Optical spectrum of the generated pulses. The 3 dB spectral width is 14 nm at 1562 nm. (b) Mode-locked pulse train with a period of 19.6 ns. (c) Intensity autocorrelation trace with 185 fs pulse duration. (d) RF spectrum with 95 dB SNR measured with 10 Hz RBW.

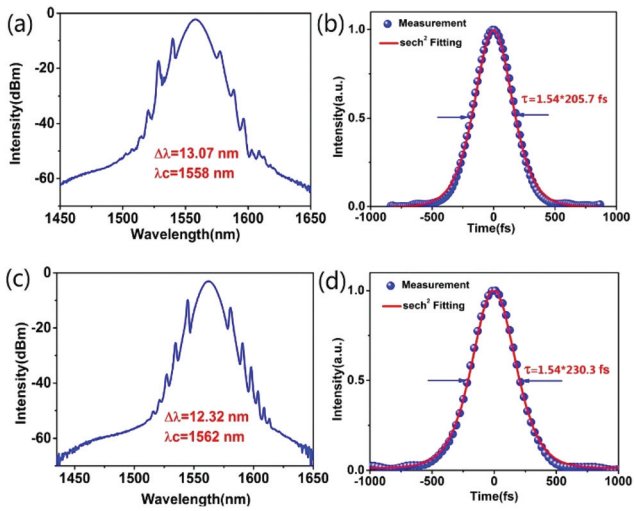

Fig. 8 Optical spectra and pulse durations. (a) and (b) correspond to the 5.7 nm thick WSe_2-based SA. (c) and (d) correspond to the 11 nm thick WSe_2-based SA.

oscilloscope are used to measure the spectral and temporal characteristics, respectively. A radio frequency (RF) spectrum analyzer is applied to monitor the frequency-domain characteristics, and an optical intensity auto-correlator is used to measure the pulse duration.

To investigate the performance of WSe_2 films with different thicknesses, we couple three different WSe_2-based SAs into the fiber laser shown in Fig. 6. The maximum pump power that can be realized in the experiment is 650 mW. We measure the characteristics of pulses through the 20% optical coupler (OC).

The performance of the pulse is summarized in Fig. 7 when we couple the 1.5 nm thick WSe_2 into the loop. Fig. 7(a) shows a typical soliton spectrum with obvious Kelly spectral sidebands, which is the result of the interactions of the dispersion and nonlinearity. The 3 dB bandwidth is 14 nm, and is centered at 1562 nm. This spectrum corresponds to a transform-limited pulse of 182 fs. The uniform mode-locked pulse train without the peak modulation is obtained with a 500 MHz oscilloscope, as shown in Fig. 7(b). The period of the mode-locked pulse train is 19.6 ns, as expected from the fiber cavity length. Assuming a $sech^2$ temporal profile, the output pulse is measured to be 185 fs as shown in Fig. 7(c). This is the shortest pulse duration for a given spectral width, which also confirms the soliton-like operation. In such a regime, the pulse shaping is initiated by the WSe_2 SA. To study the operation stability, we measure the RF spectrum. A 95 dB SNR is observed, indicating high quality in terms of good mode-locking stability. The repetition rate of the EDF laser is about 58.8 MHz at a RBW of 10 Hz in Fig. 7(d).

Then the length of the cavity is kept constant, and the WSe_2 film with a thickness of 5.7 nm is used to prepare the SA. The spectrum and the pulse duration of the mode-locked fiber laser are 13.07 nm and 205.7 fs in Fig. 8(a) and (b), respectively. Similarly, the 11 nm thick WSe_2 film applies in the mode-locked fiber laser successfully. The corresponding spectrum and pulse duration are 12.32 nm and 230.3 fs in Fig. 8(c) and (d), respectively. After the comparisons among different thickness WSe_2 films, we have found that the thinner WSe_2 film has a certain advantage in the realization of short pulses. As the modulation depth of the WSe_2-based SA increases, the pulse narrowing effect of the SA gets better. The maximum optical damage threshold of the 1.5 nm thick, 5.7 nm thick and 11 nm thick WSe_2 SAs are respectively 4.012 mJ cm^{-2},

Table 1 Comparison of mode-locked EDF lasers with SAs based on different nonlinear optical materials

Materials	Preparation method	Pulse duration (fs)	SNR (dB)	Modulation depth (%)	Output power (mW)	Ref.
WS_2	PLD	246	92	17.2	18	25
$MoSe_2$–PVA	LPE	737	61.9	5.4	3.96	47
WSe_2–PVA	LPE	1250	50	0.5	19	50
CNTs	—	97.5	—	15.8	3.93	56
Graphene	CVD	88	65	11	1.5	57
GO	Marcano	613	69	1.4	0.83	58
Bi_2Se_3–PVA	Polyol	360	56	5.2	0.86	59
BPs	ME	272	65	4.6	0.5	60
MoS_2	LI	521	54	—	0.79	61
WSe_2	CVD	185	95	52.38	30	This work

4.2393 mJ cm^{-2} and 4.4934 mJ cm^{-2}, which are higher than the commercially available SESAMs (500 μJ cm^{-2}).

In addition, the pulse duration of 185 fs reaches the best level among all the TMDs-based mode-locked lasers. From Table 1, we can see that the pulse duration in our fiber laser is shorter than that in most of the mode-locked fiber lasers. Moreover, the modulation depth, SNR and output power have shown significantly better results than earlier reports.

Conclusions

Three kinds of WSe_2 films with different thicknesses have been prepared using the chemical vapor deposition method, and successfully incorporated into the all-fiber laser to generate mode-locked pulses. Compared with WSe_2–PVA films synthesized *via* the liquid-phase exfoliation method, the few-layer WSe_2 films transferred onto the end face of optical fiber ferrules have better optical properties in terms of the laser induced damage threshold and modulation depth. And we have obtained the WSe_2 SAs with different modulation depths by controlling the thickness of the WSe_2 films. Moreover, the pulse duration of 185 fs based on the 1.5 nm thick WSe_2 is the shortest pulse duration generated from all-fiber lasers with TMD SAs. These results indicate that layered WSe_2 is a prospective saturable absorption material to improve the modulation depth for generating stable high power ultrashort mode-locked pulses.

Conflicts of interest

The authors declare that there are no conflicts to declare.

Acknowledgements

We acknowledge the financial support from the National Natural Science Foundation of China (NSFC) (Grant No. 11674036); the Beijing Youth Top-notch Talent Support Program (Grant No. 2017000026833ZK08); and the Fund of State Key Laboratory of Information Photonics and Optical Communications (Beijing University of Posts and Telecommunications, Grant No. IPOC2016ZT04, IPOC2017ZZ05).

References

1 Q. L. Bao, H. Zhang, Y. Wang, Z. H. Ni, Y. L. Yan, Z. X. Shen, K. P. Loh and D. Y. Tang, *Adv. Funct. Mater.*, 2009, **19**, 3077–3083.
2 H. Zhang, S. Virally, Q. L. Bao, K. P. Loh, S. Massar, N. Godbout and P. Kockaert, *Opt. Lett.*, 2012, **37**, 1856–1858.
3 Q. L. Bao and K. P. Loh, *ACS Nano*, 2012, **6**, 3677–3694.
4 H. Zhang, D. Y. Tang, L. M. Zhao, Q. L. Bao and K. P. Loh, *Opt. Express*, 2009, **17**, 17630–17635.
5 Z. Sun, T. Hasan, F. Torrisi, D. Popa, G. Privitera, F. Wang, F. Bonaccorso, D. M. Basko and A. C. Ferrari, *ACS Nano*, 2010, **4**, 803–810.
6 Z. Luo, M. Zhou, J. Weng, G. Huang, H. Xu, C. Ye and Z. Cai, *Opt. Lett.*, 2010, **35**, 3709–3711.
7 M. Zhang, E. J. R. Kelleher, F. Torrisi, Z. Sun, T. Hasan, D. Popa, F. Wang, A. C. Ferrari, S. V. Popov and J. R. Taylor, *Opt. Express*, 2012, **20**, 25077–25084.
8 A. P. Luo, P. F. Zhu, H. Liu, X. W. Zheng, N. Zhao, M. Liu, H. Cui, Z. C. Luo and W. C. Xu, *Opt. Express*, 2014, **22**, 27019–27025.
9 Z. Q. Luo, D. D. Wu, B. Xu, H. Y. Xu, Z. P. Cai, J. Peng, J. Weng, S. Xu, C. H. Zhu, F. Q. Wang, Z. P. Sun and H. Zhang, *Nanoscale*, 2016, **8**, 1066–1072.
10 S. Lu, C. Zhao, Y. Zou, S. Chen, Y. Chen, Y. Li, H. Zhang, S. Wen and D. Tang, *Opt. Express*, 2013, **21**, 2072–2082.
11 H. Chen, Y. Chen, J. Yin, X. Zhang, T. Guo and P. Yan, *Opt. Express*, 2016, **24**, 16287–16296.
12 H. Liu, X. W. Zheng, M. Liu, N. Zhao, A. P. Luo, Z. C. Luo, W. C. Xu, H. Zhang, C. J. Zhao and S. C. Wen, *Opt. Express*, 2014, **22**, 6868–6873.
13 P. Yan, R. Lin, S. Ruan, A. Liu and H. Chen, *Opt. Express*, 2015, **23**, 154–164.
14 J. J. McFerran, *Appl. Opt.*, 2009, **48**, 2752–2759.
15 M. E. Fermann and I. Hartl, *Nat. Photonics*, 2013, **7**, 868–874.
16 Z. Jiang, C. B. Huang, D. E. Leaird and A. M. Weiner, *Nat. Photonics*, 2007, **1**, 463–467.
17 F. Wang, A. G. Rozhin, V. Scardaci, Z. Sun, F. Hennrich, I. H. White, W. I. Milne and A. C. Ferrari, *Nat. Nanotechnol.*, 2008, **3**, 738–742.
18 J. Sotor, G. Sobon, M. Kowalczyk, W. Macherzynski, P. Paletko and K. M. Abramski, *Opt. Lett.*, 2015, **40**, 3885–3888.
19 V. J. Matsas, T. P. Newson, D. J. Richardson and D. N. Payne, *Electron. Lett.*, 1992, **28**, 1391–1393.
20 D. J. Richardson, R. I. Laming, D. N. Payne, V. Matsas and M. W. Phillips, *Electron. Lett.*, 1991, **27**, 542–544.
21 I. N. Duling, *Opt. Lett.*, 1991, **16**, 539–541.
22 A. Martinez and Z. Sun, *Nat. Photonics*, 2013, **7**, 842–845.
23 S. Y. Set, H. Yaguchi, Y. Tanaka and M. Jablonski, *J. Lightwave Technol.*, 2004, **22**, 51–56.
24 Y. Chen, G. B. Jiang, S. Q. Chen, Z. N. Guo, X. F. Yu, C. J. Zhao, H. Zhang, Q. L. Bao, S. C. Wen, D. Y. Tang and D. Y. Fan, *Opt. Express*, 2015, **23**, 12823–12833.
25 W. J. Liu, L. H. Pang, H. N. Han, K. Bi, M. Lei and Z. Y. Wei, *Nanoscale*, 2017, **9**, 5806–5811.
26 K. Wang, J. Wang, J. Fan, M. Lotya, A. O'Neill, D. Fox, Y. Feng, X. Zhang, B. Jiang, Q. Zhao, H. Zhang, J. N. Coleman, L. Zhang and W. J. Blau, *ACS Nano*, 2013, **7**, 9260–9267.
27 R. Khazaeizhad, S. H. Kassani, H. Jeong, D. I. Yeom and K. Oh, *Opt. Express*, 2014, **22**, 23732–23742.
28 K. F. Mak and J. Shan, *Nat. Photonics*, 2016, **10**, 216–226.

29 Q. H. Wang, K. Kalantar-Zadeh, A. Kis, J. N. Coleman and M. S. Strano, *Nat. Nanotechnol.*, 2012, **7**, 699–712.
30 B. Radisavljevic, A. Radenovic, J. Brivio, V. Giacometti and A. Kis, *Nat. Nanotechnol.*, 2011, **6**, 147–150.
31 M. Chhowalla, H. S. Shin, G. Eda, L. J. Li, K. P. Loh and H. Zhang, *Nat. Chem.*, 2013, **5**, 263–275.
32 M. Pumera, Z. Sofer and A. Ambrosi, *J. Mater. Chem. A*, 2014, **2**, 8981–8987.
33 X. Huang, Z. Zeng and H. Zhang, *Chem. Soc. Rev.*, 2013, **42**, 1934–1946.
34 J. Kang, W. Liu, D. Sarkar, D. Jena and K. Banerjee, *Phys. Rev. X*, 2014, **4**, 031005.
35 K. Wang, Y. Feng, C. Chang, J. Zhan, C. Wang, Q. Zhao, J. N. Coleman, L. Zhang, W. J. Blau and J. Wang, *Nanoscale*, 2014, **6**, 10530–10535.
36 Y. Zhang, T. R. Chang, B. Zhou, Y. T. Cui, H. Yan, Z. K. Liu, F. Schmitt, J. Lee, R. Moore, Y. L. Chen, H. Lin, H. T. Jeng, S. K. Mo, Z. Hussain, A. Bansil and Z. X. Shen, *Nat. Nanotechnol.*, 2014, **9**, 111–115.
37 S. Wang, H. Yu, H. Zhang, A. Wang, M. Zhao, Y. Chen, L. Mei and J. Wang, *Adv. Mater.*, 2014, **26**, 3538–3544.
38 D. Mao, B. Du, D. Yang, S. Zhang, Y. Wang, W. Zhang, X. She, H. Cheng, H. Zeng and J. Zhao, *Small*, 2016, **12**, 1489–1497.
39 R. Lv, J. A. Robinson, R. E. Schaak, D. Sun, Y. Sun, T. E. Mallouk and M. Terrones, *Acc. Chem. Res.*, 2015, **48**, 56–64.
40 H. Y. Shi, R. S. Yan, S. Bertolazzi, J. Brivio, B. Gao, A. Kis, D. Jena, H. G. Xing and L. B. Huang, *ACS Nano*, 2013, **7**, 1072–1080.
41 K. G. Zhou, M. Zhao, M. J. Chang, Q. Wang, X. Z. Wu, Y. L. Song and H. L. Zhang, *Small*, 2015, **11**, 694–701.
42 G. Cunningham, M. Lotya, C. S. Cucinotta, S. Sanvito, S. D. Bergin, R. Menzel, M. S. P. Shaffer and J. N. Coleman, *ACS Nano*, 2012, **6**, 3468–3480.
43 D. Mao, Y. Wang, C. Ma, L. Han, B. Jiang, X. Gan, S. Hua, W. Zhang, T. Mei and J. Zhao, *Sci. Rep.*, 2015, **5**, 7965.
44 H. Zhang, S. B. Lu, J. Zheng, J. Du, S. C. Wen, D. Y. Tang and K. P. Loh, *Opt. Express*, 2014, **22**, 7249–7260.
45 X. Fu, J. Qian, X. Qiao, P. Tan and Z. Peng, *Opt. Lett.*, 2014, **39**, 6450–6453.
46 S. Zhang, N. Dong, N. McEvoy, M. O'Brien, S. Winters, N. C. Berner, C. Yim, Y. Li, X. Zhang, Z. Chen, L. Zhang, G. S. Duesberg and J. Wang, *ACS Nano*, 2015, **9**, 7142–7150.
47 J. Koo, J. Park, J. Lee, Y. M. Jhon and J. H. Lee, *Opt. Express*, 2016, **24**, 10575–10589.
48 S. Bikorimana, P. Lama, A. Walser, R. Dorsinville, S. Anghel, A. Mitioglu and L. Kulyuk, *Opt. Express*, 2016, **24**, 20685–20695.
49 C. S. Guo, B. H. Chen, H. Wang, X. Y. Zhang, J. Wang, K. Wu and J. Chen, *IEEE Photonics J.*, 2016, **8**, 1503612.
50 D. Mao, X. She, B. Du, D. Yang, W. Zhang, K. Song, X. Cui, B. Jiang, T. Peng and J. Zhao, *Sci. Rep.*, 2016, **6**, 23583.
51 L. Tao, F. C. Meng, S. D. Zhao, Y. L. Song, J. X. Yu, X. J. Wang, Z. G. Liu, Y. Wang, B. S. Li, Y. Wang and Y. Sui, *Nanoscale*, 2017, **9**, 4898–4906.
52 H. Sahin, S. Tongay, S. Horzum, W. Fan, J. Zhou, J. Li, J. Wu and F. M. Peeters, *Phys. Rev. B: Condens. Matter Mater. Phys.*, 2013, **87**, 165409.
53 H. Li, J. Wu, Z. Yin and H. Zhang, *Acc. Chem. Res.*, 2014, **47**, 1067–1075.
54 R. F. Wei, H. Zhang, X. L. Tian, T. Qiao, Z. L. Hu, Z. Chen, X. He, Y. Z. Yu and J. R. Qiu, *Nanoscale*, 2016, **8**, 7704–7710.
55 M. Sheik-Bahae, A. A. Said and E. W. Van-Stryland, *Opt. Lett.*, 1989, **14**, 955–957.
56 J. Wang, Z. Cai, P. Xu, G. Du, F. Wang, S. Ruan, Z. Sun and T. Hasan, *Opt. Express*, 2015, **23**, 9947–9958.
57 J. Sotor, I. Pasternak, A. Krajewska, W. Strupinski and G. Sobon, *Opt. Express*, 2015, **23**, 27503–27508.
58 J. Boguslawski, J. Sotor, G. Sobon, R. Kozinski, K. Librant, M. Aksienionek, L. Lipinska and K. M. Abramski, *Photonics Res.*, 2015, **3**, 119–124.
59 K. X. Li, Y. R. Song, Z. H. Yu, R. Q. Xu, Z. Y. Dou and J. R. Tian, *Laser Phys. Lett.*, 2015, **12**, 105103.
60 J. Sotor, G. Sobon, W. Macherzynski, P. Paletko and K. M. Abramski, *Appl. Phys. Lett.*, 2015, **107**, 051108.
61 R. Khazaeinezhad, S. H. Kassani, H. Jeong, T. Nazari, D. Yeom and K. Oh, *IEEE. Photon. J.*, 2015, **7**, 1500109.